Proceedings of the ASME 2014 International Mechanical Engineering Congress and Exposition
IMECE2014
November 14-20, 2014, Montreal, Quebec, Canada

IMECE2014-39568

TRIBOLOGICAL STUDY OF MAGNESIUM ALLOYS FOR IMPLANT APPLICATIONS

Paul McGhee[a], Devdas Pai[a], Sergey Yarmolenko[a], Zhigang Xu[a], Sudheer Neralla[b], Yongjun Chen[a]
[a] NSF Engineering Research Center for Revolutionizing Metallic Biomaterials
North Carolina A&T State University
Greensboro, NC 27411

[b] Jet-Hot High Performance Coating
Burlington, NC 27215

ABSTRACT
Magnesium and its alloys have been found to potential candidates for biodegradable implant applications. However, magnesium and its alloys are broadly known to have poor tribological properties, but detailed specifics on wear performance are scarce. This research investigates the tribological characteristics on Mg-Zn-Ca-RE alloys and pure magnesium under as-cast and extruded conditions. Pure magnesium and Mg-Zn-Ca-RE alloys were hot extruded at 350^{o}C and 400^{o}C. Magnesium and Mg-Zn-Ca-Re alloy were also cast at 350^{o}C and heat treated at 510^{o}C. Directional wear properties were investigated using a CETR-UMT 2 microtribometer under unlubricated conditions in a reciprocating configuration for 120 cycles, with normal loads ranging from 0.5N-2.5N. Wear tests were conducted in directions: cross-sectional, longitudinal (along the extrusion direction) and transverse direction (perpendicular to the extrusion direction). Wear properties and friction properties were analyzed using a microtribometer, a mechanical stylus profiler, and microindentation. Surface morphology and microstructure were characterized using optical microscopy, scanning electron microscopy, and optical profilometry. The results show a lower wear rate in the transverse and cross-sectional direction compared to the longitudinal direction.

Keywords: Reciprocating wear, magnesium alloy Mg-Zn-Ca-RE, extrusion, as-cast

1. INTRODUCTION
Biodegradable materials have become the focus of research in the development of implant devices in medical areas ranging from cardiovascular, dental, reconstructive surgery, and orthopedics applications [1]. Biomaterials must satisfy design and biological requirements for successful use in orthopedic devices. These devices are implanted into the human body as supports or to replace an important bodily function, such as screws and fixation plates to repair bone fractures [2-4]. Orthopedic biomaterials must successfully function inside the human body, which is a highly corrosive environment that is sensitive to foreign bodies. Biomaterials must be biocompatible to perform within the environment without triggering any foreign body reaction [5] from the body's natural defenses, and produce corrosion and wear-related degradation products[6] that are not toxic. Mechanical properties of the biomaterial must be carefully selected to provide sufficient stability and strength to support the healing fracture during the expected time of recovery and bone generation. In orthopedic applications, the matching of mechanical properties of the biomaterial and biological material such as bone are very important because mismatching of the properties can produce negative stress-shielding effects that result in the resorption of new bone growth and a reduction in implant stability [7] that would require revision surgery. Biomaterials should not have similar mechanical properties to its surrounding tissue, but it should degrade at a rate that matches the rate of healing of the tissue [1, 8].

Metallic biomaterials have been the material of choice for load-bearing applications [3, 7, 9]. Stainless steel, cobalt-chromium alloys, titanium and titanium alloys are currently approved and used for permanent internal fixation due to their

high mechanical strength, fracture toughness, and corrosion resistance. The potential drawbacks to using biomaterial within the human body include the release of toxic ions/particles from corrosion products which, trigger the body's foreign body response, stress shielding phenomena due to the mismatch of mechanical properties, which cause the implant stability to become less stable, and the need for a second surgery to remove implant material after the body recovers from fracture, which would increase the costs of health care and possible increase morbidity to the patient. [4, 6, 7, 10-12].

Magnesium (Mg) and its alloys have become the research focus as candidates for biodegradable implant applications [13]. Magnesium and magnesium alloys are exceptionally light-weight metals with density between 1.74-2.0 g/cm^3 and elastic modulus ranging from 41-45 GPa. These numbers are similar to those for human bones materials (1.8 - 2.1 g/cm^3, 3-20 GPa) [6-8, 14-16] as compared to traditional non-degradable implant material like stainless steel, Co-Cr alloys and Ti alloys. The corrosion product of Mg is non-toxic. Mg is beneficial to the human body since it's the fourth most abundant cation in the body. It is found stored in bone tissue, and promotes bone growth [7, 8, 17]. Magnesium is a cofactor for many enzymes and stabilizes the structure of DNA and RNA [7, 8, 18]. Low corrosion and wear resistance are major setbacks of pure Mg which can affect the mechanical integrity of the implant materials [18-21]. The corrosion behavior and the mechanical properties of Mg can be improved through alloying and protective coating techniques ensuring that material remains biocompatible [7, 17, 19]. Modification of the material's surface and composition to retard the corrosion rate is desirable to allow sufficient time for the healing tissue to gain strength as the implant gradually degrades, losing its ability to support. This controlled biodegradability is what would eliminate the need for secondary surgery.

Interest of Mg alloys continues to rise, but friction and wear behavior data available for these alloys are very limited. The literature reports on the tribological properties for a few magnesium alloys such as AZ91 [21, 22], ZE41A [20, 21, 23, 24], AZ61 [25], Mg-11Y-5Gd-2Zn alloy [21], and Mg-Zn-Y alloy [20, 21, 26]. Despite the number of tribological studies conduct on magnesium alloy, there is limited information on the wear behavior of magnesium alloy containing zinc (Zn), calcium (Ca), or rare earth (RE) simultaneously.

Mg-Zn-Ca-RE (MZCR) alloys investigated in this study possess attractive mechanical properties due to the addition of alloy elements. Alloys element such as Zn, Mn, Ca, and small amount of RE used within the human body to retard the degradation of the Mg [17]. Ca and Zn are important elements found in the human body. Mg alloy with the addition of Ca increase biocompatibility and Zn increase mechanical properties and corrosion resistance of magnesium alloys [17, 27]. Mg-Zn-Ca alloy possess fine participates in the matrix that contributes to the high strength and hardness [28].

The purpose of this work is to study the directional wear properties of pure-Mg and MZCR under as-cast conditions and extruded Mg and MZCR alloys under extrusion ratio of 10 (ER10) on cross-sectional and longitudinal cuts. Wear properties were analyzed parallel and perpendicular to the extrusion direction of the longitudinal cut.

Table 1
Comparison of biomaterial and natural bone

Properties	Natural Bone	Mg	Ti alloy	Co-Cr alloy	Stainless Steel
Density (g/cm^3)	1.8-2.1	1.74-2.0	4.4-4.5	8.3-9.2	7.9-8.1
Elastic Modulus (GPa)	3-20	41-45	110-117	230	189-205
Compressive. Yield Strength	130-180	65-100	758-1117	450-1000	170-310
Fracture Toughness (MPam$^{1/2}$)	3-6	15-40	55-115	N/A	50-200

**Compiled from references [6-8, 14, 16, 29]

2. EXPERIMENTAL DETAILS

2.1 Sample Preparation

Magnesium (99.97%) and MZCR were machined under three conditions: as-cast (pure Mg), as-cast solution heat treated (MZCR-T4) and extrusion under an extrusion ratio of 10. As-cast magnesium and MZCR were cast at temperature of 350°C and heat treated at 510°C. Mg was extruded at 350°C and MZCR at 410°C with extrusion ratio of 10 at 1 mm/s resulting in rods with diameters of 12mm. The extruded specimens were cut using a diamond disc precision cutter. The specimen was cut normal and parallel to the specimen's extrusion direction resulting in cross-sectional specimen (12 mm diameter and 8mm thickness) and longitudinal section (8mm diameter and 4mm thickness). Contact surfaces were polished using 9 μm, 5 μm, 3 μm, 1 μm alumina using lubricant. Using a Wyko RST-500 optical profiler the average surface roughnesses of Mg and MZCR were measured to be about 0.15μm and 0.18μm respectively. The specimens were etched with picric acid to reveal and add contrast to the grain boundaries.

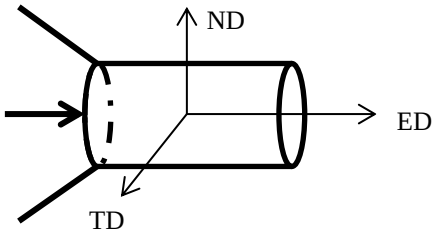

Fig. 1 Schematic illustration of the extrusion process of metals.

Microstructures were characterized using optical (Zeiss Axiovert-10) and scanning electron microscopy (SEM-Hitachi S-3000N).The microstructure of the as-cast MZCR alloys observed by optical microscopy is shown in Fig. 2. Fig. 2a show the polycrystalline heat treated MZCR. The average grain size of the as-cast of the heat treated MZCR is 25.1±14.8 μm. Fig. 2b and Fig. 2c is the micrographs of the longitudinal section and cross-section of the extruded MZCR alloy, respectively. After extrusion, the grain size of the longitudinal section was 2.5 ± 2.2 μm and the cross-section was 3.3 ± 2.8 μm.

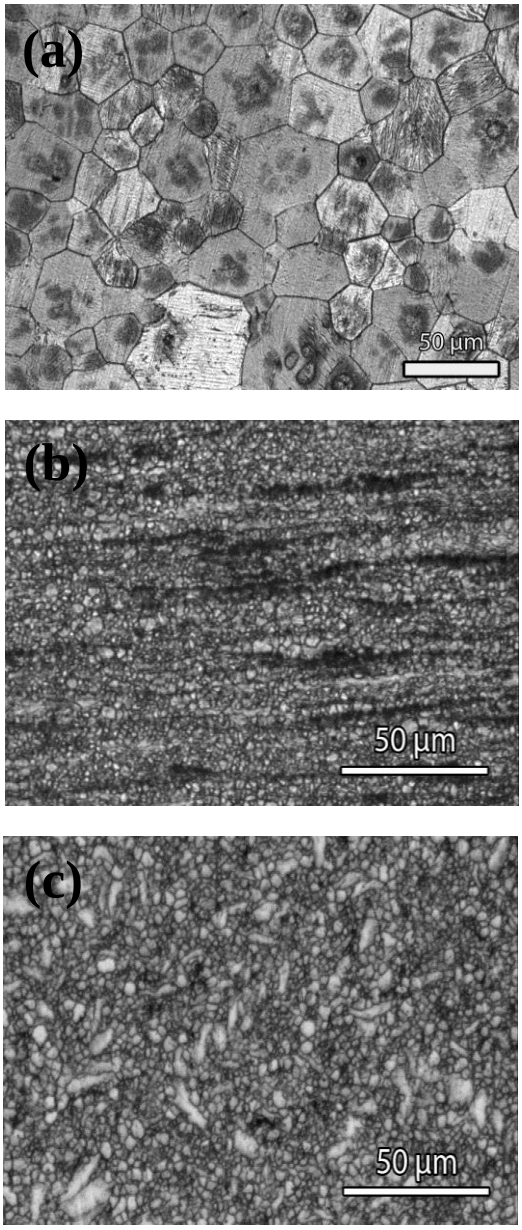

Fig.2 Optical micrograph of the a) as-cast MZCR (T4) and extruded MZCR b) longitudinal and c) cross-section.

2.2 Reciprocating Wear Test

Reciprocating wear tests were conducted on a microtribometer (CETR-UMT-2) to assess the wear and friction characteristics of the Mg and MZCR alloys. Testing was done under dry conditions against a sapphire sphere counter- face. The sapphire sphere geometry consists of a diameter of 3.97 mm with a Vickers hardness of 2500. The sapphire specimen was cleaned in an ultrasonic cleaner with distilled water for 30 minutes to remove wear debris. Test specimen were etched with picric acid (for microstructural analysis) and cleaned with isopropanol. Wear tests were conducted for 120 cycles (10 minutes test duration) under loads of 0.5 N, 1.0 N, 1.5 N, 2.0 N, and 2.5 N. Frictional force, normal force, shear force, height/depth, and coefficient of friction were monitor and recorded. Wear tests were executed on the sample's surface on cross-section and longitudinal section. The longitudinal section's surface experiences wear in the extrusion direction and transverse direction shown in Fig. 3. Each test was replicated three times to ensure reproducibility and then averaged in order to determine the wear rate.

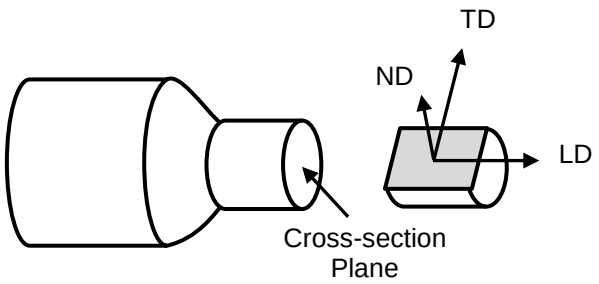

Fig.3 Schematic of extruded specimen's coordinates system. Wear test was conducted on longitudinal section in the extrusion and transverse direction and cross-sectional section in the normal and transverse direction plane.

A mechanical stylus (KLA-Tencor Alpha-Step IQ, tip radius of 5 μm) was used to record the profile of the worn surface, recording information regarding width, depth, and area of the wear tracks. Wear tracks were measured 10 times at equidistant location depending on the stroke length of the wear tracks. Wear volume was calculated by the measured area of the wear profile multiply by the sliding distance. Wear rates were calculated by dividing wear volume by the sliding distance under Archard's law [20, 24, 30-32]:

$$\dot{W} = \frac{V}{x} = K\frac{L}{H} = \kappa L \quad (1)$$

where, $\dot{W}$ is the wear rate (mm^3/m), V is the wear volume (mm^3), x is the sliding distance (m), K s the wear coefficient(dimensionless), H is the hardness (GPa), L is the load (N), κ is the specific wear rate (mm^3/N-m).

The worn specimen's morphology and wear debris were characterized using optical (Zeiss Axiovert-10) and SEM (Hitachi S-3000N).

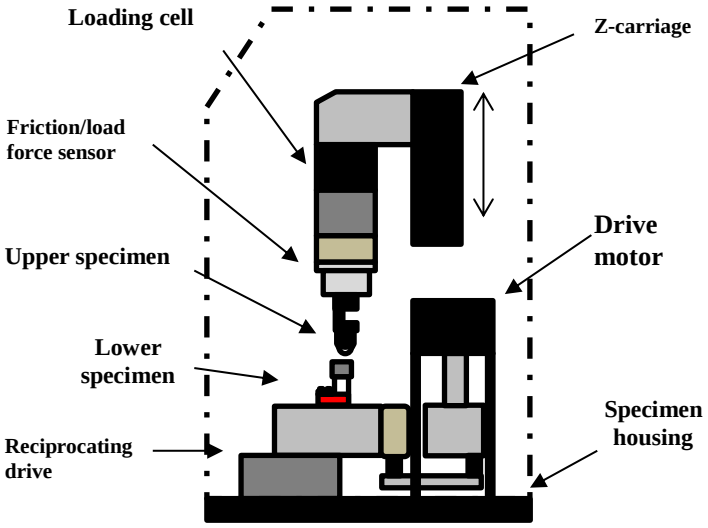

Fig. 4 Schematic of tribometer with reciprocating configuration.

2.3 Microindentation Test

Microindentation tests were carried out using an micro-hardness tester (LECO M-400-H1) to investigate the hardness of the magnesium and Mg-Zn-Ca-RE alloys. Samples were prepared under the exact condition as the wear samples. Cross-sectional and longitudinal section was tested. Vickers microindentation tests were conducted for 30 s per indent using an indentation force of 2.94N ($HV_{0.3}$) with indent spacing of 30 µm. At least 20 indentations were carried out per sample. The hardness of the specimen was calculated according to the definition of the geometry of the indent. Well-defined indents were calculated based on ASTM standard E384-11[33]. Skewed indents were analyzed through Image Pro Plus software. Skewed indents area were calculated based on the traced perimeter and hardness was calculated by dividing load over area multiplied by 10^3.

3. RESULTS AND DISCUSSION

***3.1** Wear Behavior*

Wear tests were conducted as indicated in the experimental section. The variation in volumetric wear rates and coefficient of friction for as-cast Mg and MZCR-T4 are plotted against the applied normal load in Fig. 5. Volumetric wear rates are in the unit of mm^3/m by dividing wear volume by sliding distance. AC-MZCR has a higher wear rate at loads between 1.0-2.5 N compared to AC-Mg. At loads of 0.5-1.5 N, the wear rate gradually increases linearly for both AC-Mg and MZCR-T4. Changes occur in the wear rate at load of 2.0 N, where there is a slight decrease in the wear and then increase at 2.5 N. Fig. 6 displays wear volume as a function of applied normal load. It can be observed that Mg has a greater volume loss compared to the MZCR (T4) as shown in Table 2. Fig. 7 shows the wear depth as a function of volume loss of the as-cast Mg and MZCR-T4. MZCR-T4 has less wear compared to Mg, but has a higher wear depth. Depth of wear gradually increases as load increase in the range of 0.5 N-1.5 N. Maximum wear depth is achieved at applied load of 2.0 N of the MZCR alloy. Results from the microindentation shows that MZCR (T4) possesses a hardness of 0.71±0.05 GPa and Mg with a hardness of 0.45± 0.03 GPa.

Table 2
Comparison of As cast Mg and MZCR (T4)

Mat. ID	R_a (nm)	Hardness HV (GPa)	C.O.F	Specific wear rate (mm^3/N-m)	Volume loss (mm^3)
AC-Mg	183.00	0.45 (0.03)	0.37 (0.01)	5.48 (0.14)	5.29 (0.18)
AC-MZCR (T4)	52.16	0.71 (0.05)	0.32 (0.003)	6.92 (0.16)	3.82 (0.1)

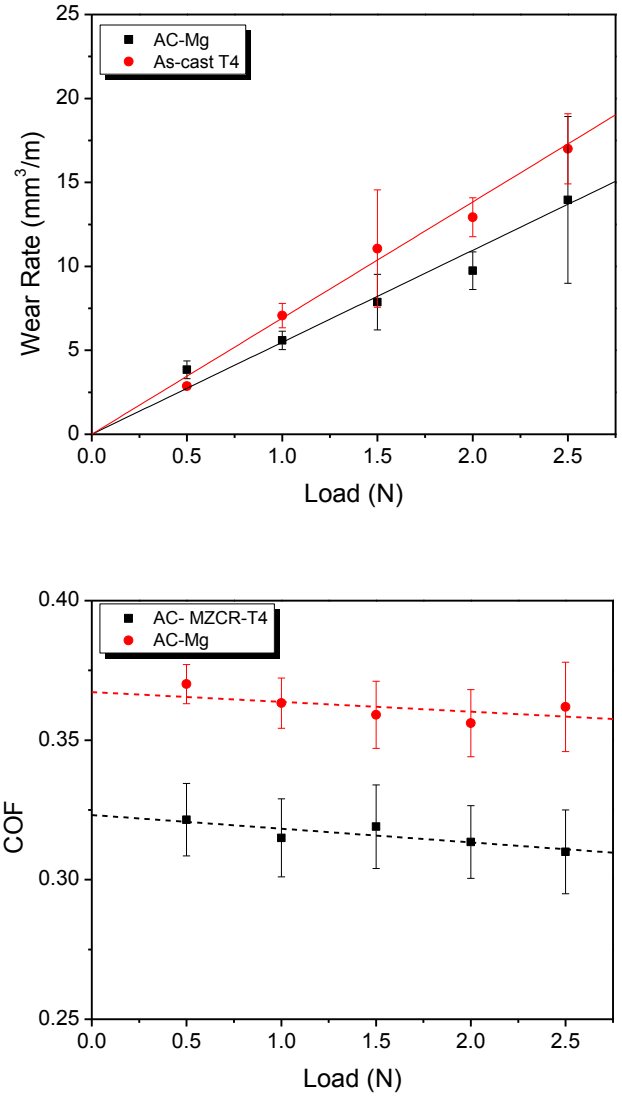

Fig. 5 Variation in terms of normal force applied of: (a) wear rate and (b) coefficient of friction.

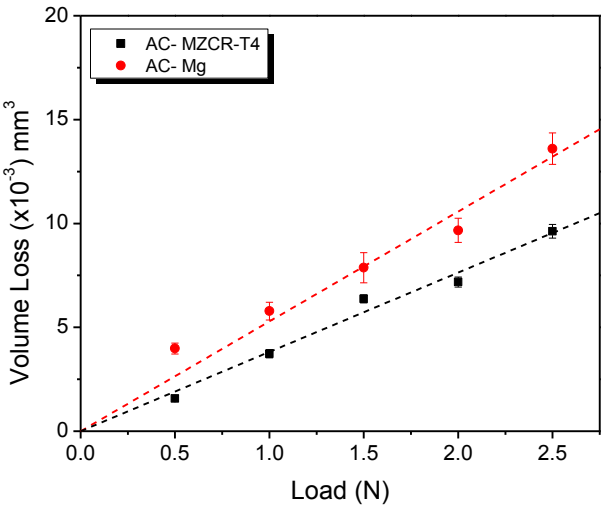

Fig. 6 Effects of volume loss as a function of applied normal load.

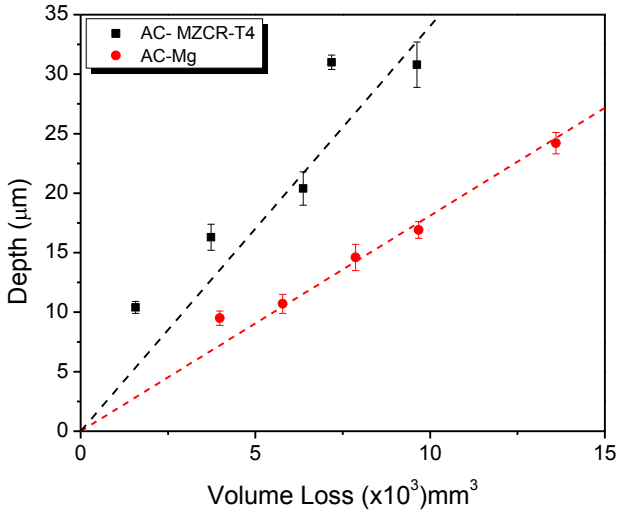

Fig. 7 Effects of wear depth as a function of volume loss.

Table 3
Comparison of directional wear of extrude Mg and MZCR

Mat. ID	R_a (nm)	Hardness HV (GPa)	COF	Specific wear rate (mm^3/N-m)	Volume loss (x10^{-3}) (mm^3)
Ex-Mg-ED	162.7	0.46(0.03)	0.37(0.01)	7.58 (0.94)	3.53(0.29)
Ex-Mg-TD	203.8	0.46(0.03)	0.35(0.01)	5.60 (0.24)	2.17(0.11)
Ex-Mg-C	148.4	0.44(0.02)	0.35(0.01)	5.29 (0.39)	2.70 (0.06)
Ex-MZCR-ED	174.3	0.70(0.02)	0.32(0.01)	5.51 (0.53)	3.56 (0.18)
Ex-MZCR-TD	64.5	0.70(0.02)	0.30(0.01)	4.39 (0.35)	3.24 (0.14)
EX-MZCR-C	73.5	0.68 (0.02)	0.31(0.01)	3.67(0.50)	4.72 (0.17)

Fig. 8 shows the wear rates of the extruded Mg and MZCR alloys plotted against the applied normal load. Table 3 shows the comparison of directional wear of the extrude Mg and MZCR alloys in terms of average roughness, hardness, coefficient of friction, specific wear rate (mm^3/m) and volume loss (mm^3) with standard deviation in parentheses. Wear rate of Mg and MZCR alloys increases as the applied load increases. Maximum wear rate occurs in extrude Mg and MZCR in the extrusion direction with specific wear rates of 7.58±0.94 and 5.51±0.53 mm^3/m, respectively. The minimum specific wear rate occurs in the transverse direction and cross-sectional plane of the MZCR alloy with wear rate of 4.39±0.35 and 3.67±0.50. Fig.9. displays the variation of coefficient of friction during wear testing of the extruded Mg and MZCR alloys as a function of the applied normal load. The average coefficient of friction is higher in the extruded Mg compared to the extruded MZCR. It can be observed that the coefficient of friction is lower for the MZCR alloy compare the extrude Mg. According to Fig. 9 it can be observe that at a applied load of 0.5 N the coefficient of friction is about 0.30 and as the load increase the coefficient of friction is decreases. The wear rate of extrude Mg decreases as the coefficient of friction decreases from 0.37 ± 0.01 to 0.35 ± 0.01. Extrude MZCR displayed similar behavior as the extrude Mg. The specific wear rate of the MZCR continues to decreases as the coefficient decreases from 0.32 ± 0.01 to 0.30 ± 0.01.

Fig.10 shows the volume loss due to wear plotted against the normal applied load. Although the wear rate of MZCR in the cross-section section is the lowest, the loss of volume is the highest. Wear in the transverse direction of the extrude Mg has the lowest volume loss of 2.17±0.11 mm^3.

3.2 Hardness

Table 3 shows the hardness value the Mg and MZCR alloy, respectively. The MZCR alloy possesses a higher hardness value as-cast and extruded compared to Mg. According to the literature [7, 8, 21] the addition of rare earth elements improves the mechanical property of the alloy. The cross-sectional plane of the Mg and MZCR has a lower hardness value compared to the longitudinal section.

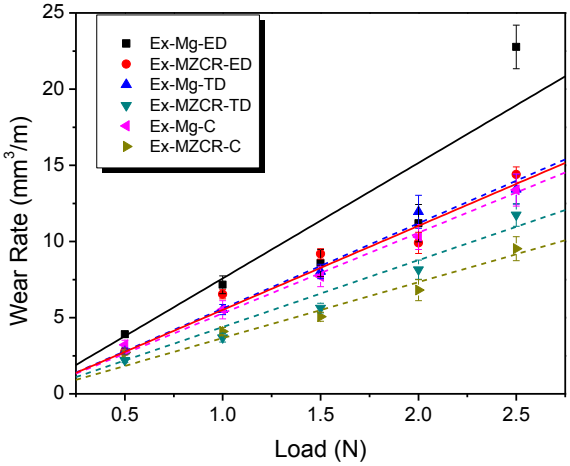

Fig. 8 Variation in the terms of normal force applied of wear rate.

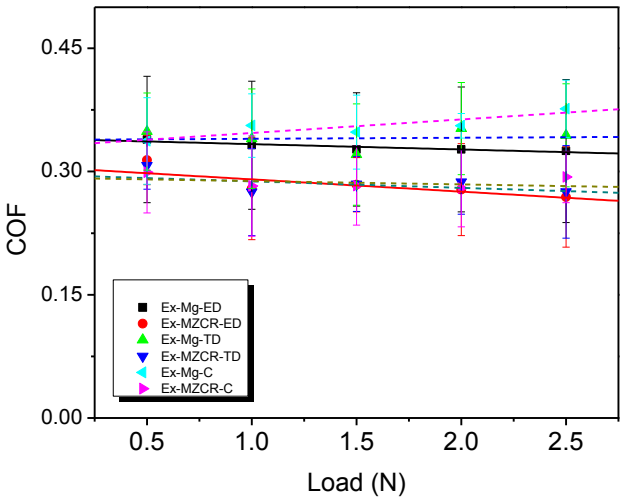

Fig. 9 Variation in the terms of normal force applied of: (a) wear rate and (b) coefficient of friction.

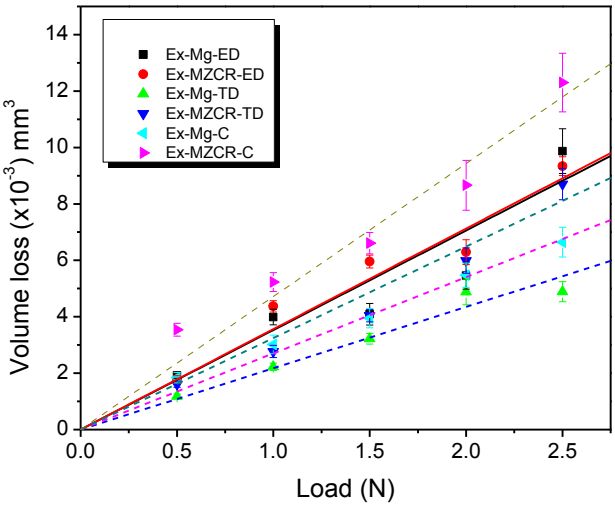

Fig. 10 Effects of volume loss as a function of applied normal load.

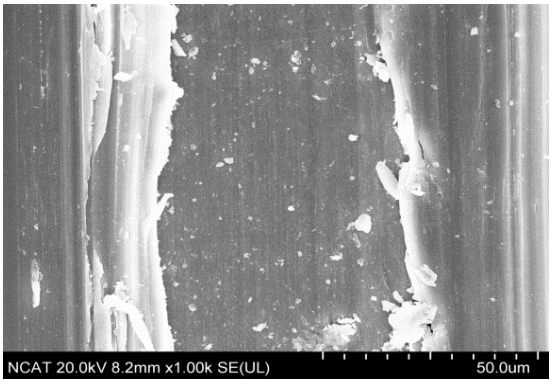

Fig. 11 SEM micrograph of the worn surface of the as-cast T4 Mg-Zn-Ca-RE.

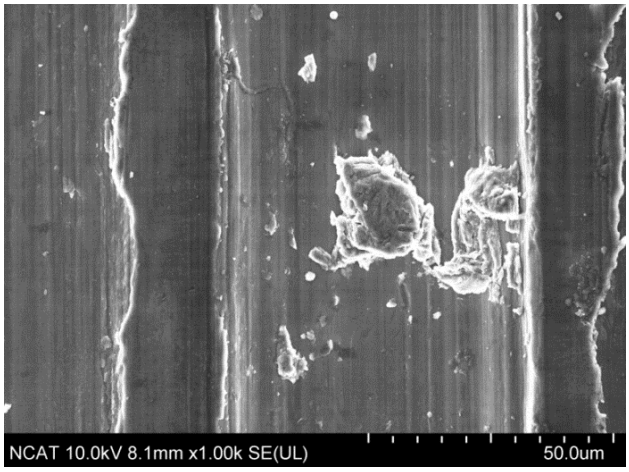

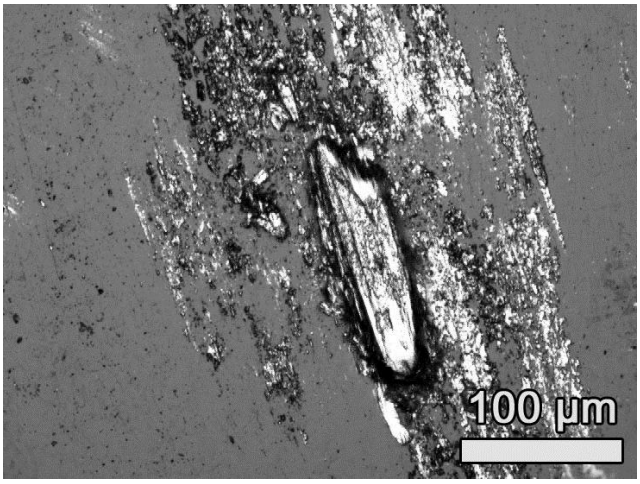

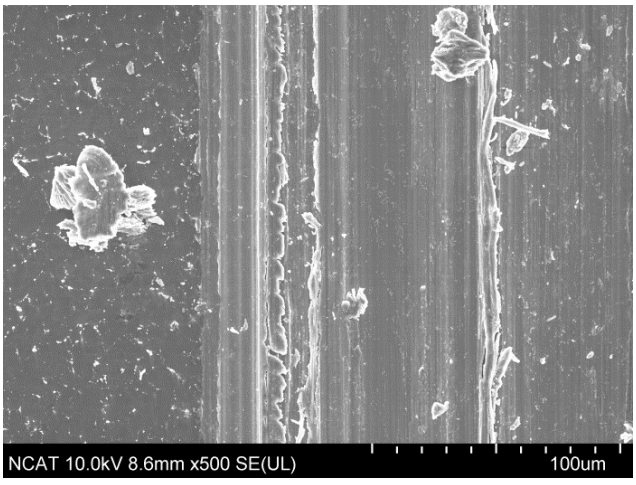

Fig. 12 SEM micrograph of wear track on the surface of a) as-cast MZCR under applied load of 1.00 N. b) Optical micrograph of the sapphire counter-face after wear testing of Mg-Zn-Ca-RE ER10 longitudinal wear under applied normal load of 2.5 N. c) Cross-section wear of extruded MZCR under applied normal load of 0.5N.

3.3 Surface Morphology

SEM and optical microscopy were carried out to analyze the worn surface morphology and wear debris collected after the wear test.

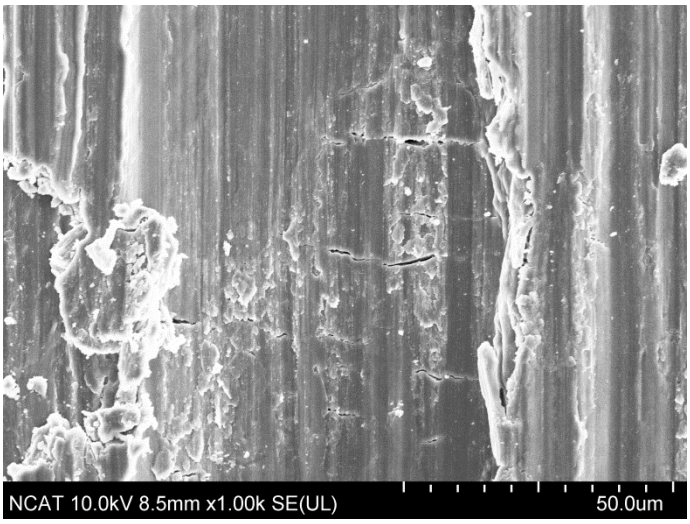

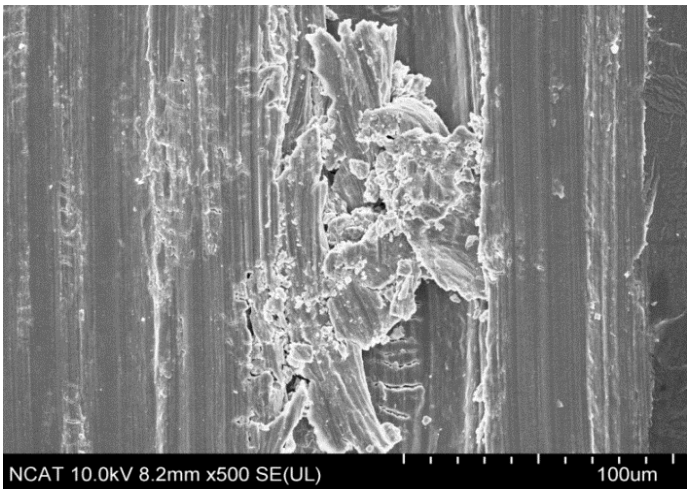

Fig.13 SEM micrographs of wear track of extrude Mg a) longitudinal wear under applied load of 1.5N. b) Cross-sectional wear under a load of 2.0N Mg-ER10 transverse wear.

3.3.1 Abrasion and Adhesion

Fig. 11 shows the surface morphology of the as-cast MZCR alloy at 2.5N applied load at 120 cycles. Fig. 12 displays the worn surfaces of the as-cast MZCR under applied load of 1.00N. Fig 12a is the worn surface of the cross-section of the extruded MZCR under applied load of 0.5N. Fig. 13 shows extrude Mg after experiencing longitudinal wear which is along the extrusion direction of the longitudinal section and cross-sectional wear under applied load of 1.5N and 2.0N, respectively,, The micrographs display evidences of grooves formed in the worn surface decorated in wear debris that are resting along the wear track. The creation of the wide groove(s) in the worn surface is proof that abrasion is one of the active mechanisms involved. Abrasion wear have been to be an active wear mechanism in both Mg and MZCR. It can also be observed from Fig. 11 that abrasive wear mechanism is evident for the material is removed from surface. According to Bayer [30, 31], abrasion wear is a wear mechanism associated with hard protuberances or particles that resulted in grooves, scratches, or indentations. In this case, the sapphire counter-face has a hardness value greater than the hardness of the Mg and MZCR resulting in ploughing of the material's surface.. Abrasion wear is the dominate wear mechanism in both material.

Fig. 12 is an optical micrograph (at magnification of 500x) of MZCR particles attached to the surface of the sapphire specimen. The micrograph shows the MZCR adhering to the surface of the sapphire thus showing evidence of adhesion wear mechanism. Bayer [30, 31] defines adhesion wear as wear occurring when one of the contacting surface is moved onto the other surface at localized sites.

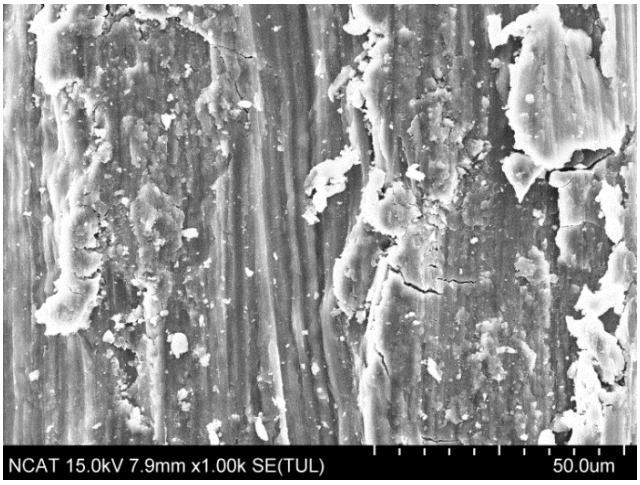

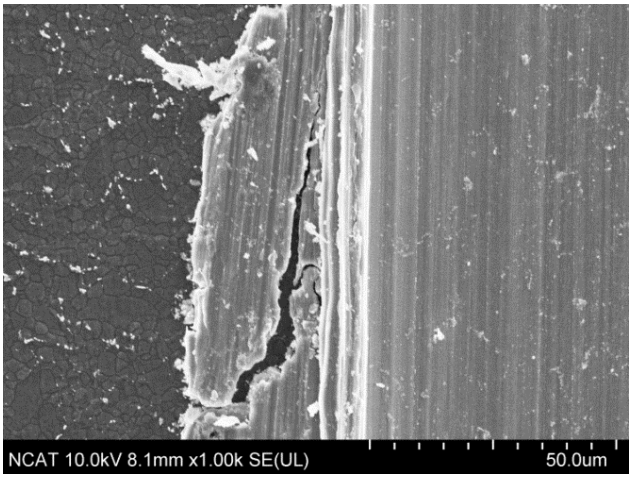

Fig. 14 SEM micrograph of worn surface of a) extruded Mg in the transverse direction under applied load of 2.5N. b) Cross-section wear track of MZCR under applied load 2.0N.

3.3.2 Delamination and Fatigue wear

Delamination can be observed in the worn surface of MZCR alloy under an applied load of 2.0N in Fig. 14b. During wear testing, particles have been smashed back into the wear track due to two-body (upper and lower specimen interaction) and three-body (upper specimen, lower specimen, and wear debris interaction) abrasion wear. Crack propagation occurred at the exterior proportion of the wear track growing towards the interior resulting detachment of material. According to [30-32] delamination occurs when a plastic flow nucleates and promotes the growth of subsurface cracks that propagate parallel to the surface, before extending out to the free surface to form platelet-like wear particles.

Cracks can be observed in the worn surface of the extruded magnesium of Fig. 13 and Fig. 14a. Crack propagations appear within and around the wear track of extruded magnesium sample indicating plastic deformation. Fatigue wear is a wear mechanism under repeated sliding, rolling, or impacting where the material's surface experiences cyclic stresses that initiate cracks wearing region [30-32]. The increase in applied normal load results in plastic deformation, which causes extensive damage to the materials.

4. Conclusions

Reciprocating wear of Mg and MZCR was tested against a sapphire specimen under testing conditions of a load range of 0.5 N-2.5 N. Studies show that the wear rate increases with the increase in applied load. Wear was investigated in the longitudinal and transverse direction of the longitudinal section and cross-section for Mg and MZCR. The wear rate of the MZCR-T4 was higher compare to the as-cast Mg. As-cast Mg has a higher rate of volume loss compared to MZCR-T4, but the MZCR-T4 has a higher wear depth. Wear rate was lower in the cross-section and in the transverse direction of the longitudinal section of the MZCR. The coefficient of friction slightly decreases (below 0.3) as the load increases in the MZCR. The wear rate decreases as the coefficient of friction decreases. MZCR has a higher hardness compared to Mg. Four different wear mechanisms were found in this study. The wear mechanisms found were abrasion, adhesion, and delamination and fatigue wear in both materials

ACKNOWLEDGMENTS

The authors acknowledge the financial support of the National Science Foundation (EEC 0812348): Engineering Research Center for Revolutionizing Metallic Biomaterials) and the Center for Advanced Materials and Smart Structures at North Carolina A&T State University for access to the necessary laboratory facilities and equipment.

REFERENCES

1. Ratner, B.D., et al., *Biomaterials Science: An Evolving , Multidisciplinary Endeavor.* 2013: p. XXXIX.
2. Wang, W., Y. Ouyang, and C.K. Poh, *Orthopaedic Implant Technology: Biomaterials from Past to Future.* Ann Acad Med Singapore, 2011. **40**(5): p. 237-44.
3. Navarro, M., et al., *Biomaterials in Orthopaedics.* J R Soc Interface, 2008. **5**(27): p. 1137-58.
4. Yetkin, H., et al., *Biodegradable Implants in Orthopaedics and Traumatology.* Turkish Journal of Medical Sciences, 2000. **30**(3): p. 297-301.
5. Ratner, B.D. and S.J. Bryant, *BIOMATERIALS: Where We Have Been and Where We are Going.* Annual Review of Biomedical Engineering, 2004. **6**(1): p. 41-75.
6. Waizy, H., et al., *Biodegradable Magnesium Implants for Orthopedic Applications.* Journal of Materials Science, 2012. **48**(1): p. 39-50.
7. Staiger, M.P., et al., *Magnesium and Its Alloys as Orthopedic Biomaterials: A Review.* Biomaterials, 2006. **27**(9): p. 1728-34.
8. Gu, X.-N. and Y.-F. Zheng, *A Review on Magnesium Alloys as Biodegradable Materials.* Frontiers of Materials Science in China, 2010. **4**(2): p. 111-115.
9. Yaszemski, M.J., *Biomaterials in Orthopedics*. 2004: M. Dekker.
10. Hench, L.L. and I. Thompson, *Twenty-First Century Challenges for Biomaterials.* J R Soc Interface, 2010. **7 Suppl 4**(Suppl 4): p. S379-91.
11. Ryan, G., A. Pandit, and D.P. Apatsidis, *Fabrication Methods of Porous Metals for use in Orthopaedic Applications.* Biomaterials, 2006. **27**(13): p. 2651-70.
12. Kraus, T., et al., *Magnesium Alloys for Temporary Implants in Osteosynthesis: In Vivo Studies of Their Degradation and Interaction with Bone.* Acta Biomater, 2012. **8**(3): p. 1230-8.
13. Seal, C.K., K. Vince, and M.A. Hodgson, *Biodegradable Surgical Implants Based on Magnesium Alloys – A Review of Current Research.* IOP Conference Series: Materials Science and Engineering, 2009. **4**: p. 012011.
14. Denkena, B. and A. Lucas, *Biocompatible Magnesium Alloys as Absorbable Implant Materials – Adjusted Surface and Subsurface Properties by Machining Processes.* CIRP Annals - Manufacturing Technology, 2007. **56**(1): p. 113-116.
15. Song, G., *Control of Biodegradation of Biocompatable Magnesium Alloys.* Corrosion Science, 2007. **49**(4): p. 1696-1701.
16. Zhang, P.B., Y. Wang, and L. Geng, *Research on Mg-Zn-Ca Alloy as Degradable Biomaterial.*
17. Shi, P., et al., *Improvement of Corrosion Resistance of Pure Magnesium in Hanks' Solution by Microarc Oxidation with Sol–Gel TiO_2 Sealing.* Journal of Alloys and Compounds, 2009. **469**(1–2): p. 286-292

18. Wu, G., et al., *Improving Wear Resistance and Corrosion Resistance of AZ31 Magnesium Alloy by DLC/AlN/Al Coating.* Surface and Coatings Technology, 2010. **205**(7): p. 2067-2073.
19. López, A.J., et al., *Dry Sliding Wear Behaviour of ZE41A Magnesium Alloy.* Wear, 2011. **271**(11-12): p. 2836-2844.
20. Hu, M.-l., et al., *Dry Sliding Wear Behavior of Cast Mg–11Y–5Gd–2Zn Magnesium Alloy.* Transactions of Nonferrous Metals Society of China, 2012. **22**(8): p. 1918-1923.
21. Aung, N.N., W. Zhou, and L.E.N. Lim, *Wear Behaviour of AZ91D Alloy at Low Sliding Speeds.* Wear, 2008. **265**(5-6): p. 780-786.
22. Selvan, S.A. and S. Ramanathan, *Dry Sliding Wear Behavior of Hot Extruded ZE41A Magnesium Alloy.* Materials Science and Engineering: A, 2010. **527**(7-8): p. 1815-1820.
23. Anbu selvan, S. and S. Ramanathan, *A Comparative Study of the Wear Behavior of As-Cast and Hot Extruded ZE41A Magnesium Alloy.* Journal of Alloys and Compounds, 2010. **502**(2): p. 495-502.
24. El-Morsy, A.-W., *Dry Sliding Wear Behavior of Hot Deformed Magnesium AZ61 Alloy as Influenced by the Sliding Conditions.* Materials Science and Engineering: A, 2008. **473**(1-2): p. 330-335.
25. An, J., et al., *Dry Sliding Wear Behavior of Magnesium Alloys.* Wear, 2008. **265**(1-2): p. 97-104.
26. Zhang, B.P., et al., *Improved Blood Compatibility of Mg-1.0Zn-1.0Ca Alloy by Micro-Arc Oxidation.* J Biomed Mater Res A, 2011. **99**(2): p. 166-72.
27. Geng, L., et al., *Microstructure and Mechanical Properties of Mg–4.0Zn–0.5Ca Alloy.* Materials Letters, 2009. **63**(5): p. 557-559.
28. Mantripragada, V.P., et al., *An Overview of Recent Advances in Designing Orthopedic and Craniofacial Implants.* J Biomed Mater Res A, 2013. **101**(11): p. 3349-64.
29. Bayer, R.G., *Engineering Design for Wear*. Vol. 176. 2004, New York: Marcel Dekker.
30. Bayer, R.G., *Mechanical Wear Prediction and Prevention*. 1994.
31. Mate, M.C., *Tribology on the Small Scale : A Bottom Up Approach to Friction, Lubrication, and Wear.* 2008: p. 333.
32. Designation, A. I. (2012). "*E384-11: Standard Test Method for Knoop and Vicker Hardness of Materials.*".